Distribution and Sources of Air pollutants in the North China Plain Based on On-Road Mobile Measurements

Yi Zhu[1], Jiping Zhang[2], Junxia Wang[1], Wenyuan Chen[1], Yiqun Han[1], Chunxiang Ye[3], Yingruo Li[1], Jun Liu[1], Limin Zeng[1], Yusheng Wu[1], Xinfeng Wang[4], Wenxing Wang[4], Jianmin Chen[4], and Tong Zhu[1,5*]

[1]State Key Joint Laboratory of Environmental Simulation and Pollution Control, College of Environmental Sciences and Engineering, Peking University, Beijing 100871, China

[2]Institute of Atmospheric Physics, Chinese Academy of Sciences, Beijing 100029, China

[3]School of Chemistry, University of Leeds, Leeds LS2 9JT, UK

[4] Environment Research Institute, School of Environmental Science and Engineering, Shandong University, Ji'nan 250100, China

[5]The Beijing Innovation Center for Engineering Science and Advanced Technology, Peking University, Beijing, China

*Corresponding Author: tzhu@pku.edu.cn

Abstract. The North China Plain (NCP) has been experiencing severe air pollution problems with rapid economic growth and urbanisation. Many field and model studies have examined the distribution of air pollutants in the NCP, but convincing results have not been achieved mainly due to a lack of direct measurements of pollutants over large areas. Here, we employed a mobile laboratory to observe the main air pollutants in a large part of the NCP from June 11 to July 15, 2013. High median concentrations of sulphur dioxide (SO_2) (12 ppb), nitrogen oxides (NO_x) ($NO+NO_2$; 452 ppb), carbon monoxide (CO) (956 ppb), black carbon (BC; 5.5 μg m^{-3}) and ultrafine particles (28350 cm^{-3}) were measured. Most of the high values, i.e., 95 percentile concentrations, were distributed near large cities, suggesting the influence of local emissions. In addition, we analysed the regional transport of SO_2 and CO, relatively long-lived pollutants, based on our mobile observations together with wind field and satellite data analyses. Our results suggested that, for border areas of the NCP, wind from outside would have a diluting effect on pollutants, while south winds would bring in pollutants accumulated during transport through other parts of the NCP. For the central NCP, the concentrations of pollutants were likely to remain at high levels, partly due to the influence of regional transport by prevalent south–north winds over the NCP and partly by local emissions.

Keywords: North China Plain, Air pollution, Distribution, On-road mobile measurements

1. Introduction

The North China Plain (NCP) is a geographically flat region in the northern part of Eastern China, which includes Beijing, Tianjin, most of Hebei, Henan and Shandong provinces, and the northern parts of Anhui and Jiangsu provinces. This region is surrounded by the Yan Mountains to the north, the Taihang Mountains to the west and the Bohai Sea to the east. The NCP covers an area of 300,000 km^2, which corresponds to about 1/32 of the total area of China, but is home to approximately 1/5 of the Chinese population. The NCP is the political, economic and agricultural centre of China. Along with rapid economic growth and urbanisation, the NCP has been experiencing severe air pollution problems (Donkelaar et al., 2010). On a global scale, the NCP is a hotspot of nitrogen dioxide (NO_2), carbon monoxide (CO), sulphate and particulate matter (PM) concentrations, according to both satellite observations and model simulations (Chin et al., 1996; Yu et al., 2010; Bechle et al., 2011; Streets et al., 2013; Bucsela et al., 2013). The concentrations of PM with an aerodynamic diameter ≤ 2.5 μm ($PM_{2.5}$) and PM_{10} in the NCP are much higher compared to other rapidly developing areas in China, such as the Yangtze River Delta (Hu et al., 2014). According to the air-quality report published by the Chinese Ministry of Environmental Protection, in 2013, 9 of the 10 most polluted cities in China were located in the NCP. Severe pollution events occur frequently in this area. Therefore, studies of air pollution problems in the NCP are essential to obtain general insights into the unique patterns of air pollution in this area and for management of emissions control policies by the government.

Over the past decade, there have been a number of investigations of air pollution in the NCP taking advantage of observation sites, aircraft measurement platforms, mobile laboratories, satellite data and air quality models. In the NCP, a network of observation sites has been built for air pollution research, mostly located in and around large cities, particularly Beijing (Xu et al., 2011; Xu et al., 2014; Wang et al., 2013; Meng et al., 2009; Shen et al., 2011; Lin et al., 2011). Variability, sources, meteorological and chemical impacts of air pollutants have been discussed by analysing these observational results. The concentrations of long-lived pollutants have been shown to be significantly influenced by wind, particularly the south and north winds, indicating that regional transport plays an important role in urban air pollution. In addition, model studies have yielded similar results in various areas of the NCP (An et al., 2007; Zhang et al., 2008; Liu et al., 2013). Satellite data have indicated that regional transport has a significant impact on the haze period in the NCP (Wang et al., 2014). Thus, it is necessary to understand regional transport to address air pollution problems in the NCP, which will require data on the distribution of air pollutants in this region.

However, observational data from a single or limited number of measurement sites cannot present the whole picture of air pollution in the NCP. A number of mobile laboratory measurements (Johansson et al. 2008; Li et al., 2009; Wang et al., 2009; Wang et al., 2011) and aircraft measurements (Huang et al. 2010; Zhang et al. 2011; Zhang et al. 2009; Zhang et al. 2014) have been used to determine pollution distributions mainly within the megacity of Beijing. There have been several reports

of model and satellite studies on the air pollution distribution in the NCP, or even the whole of China (Wei et al., 2011; Zhao et al., 2013; Ying et al., 2014; Ding et al., 2015; Ding et al., 2009). However, there are disagreements between these results, e.g., regarding the distributions of NO_2 in several hotspot areas produced from model (CMAQ) and satellite (SCIAMACHY) measurements (Shi et al., 2008). Uncertainties in model simulations such as emissions inventories, and in satellite measurements such as the influence of clouds, can only be evaluated by measuring the spatial distributions of pollutants over a large geographical area, which are still lacking.

In this study, we measured the concentrations of nitrogen oxides (NO_x), CO, sulphur dioxide (SO_2), ultrafine particles and BC with a mobile laboratory platform in the NCP. Satellite data and field wind measurements during the observation period were also used. Our specific objectives were to collect a dataset showing the spatial distribution of air pollutants in the NCP, and to characterise the regional transport within and outside the NCP. This study was performed as part of the Campaigns of Air Pollution Research in Megacity Beijing and North China Plain (CAREBeijing-NCP 2013), and involved comprehensive stereoscopic observations, including observations of two super sites, several routine sites, mobile laboratories and model work. This paper focuses on the distribution and transport of pollutants in the NCP, mainly based on data collected from a mobile platform.

2. Experimental methods

2.1 Mobile laboratory and study area

A mobile laboratory was built by our research group, details of which were previously described (Wang et al., 2009). Briefly, this mobile laboratory was constructed in 2006 on an IVECO Turin V diesel vehicle (L = 6.6 m, W = 2.4 m, H = 2.8 m; payload = 2.7 metric tonnes). Instrumentation was powered by two sets of uninterruptible power systems (UPS), consisting of three series of 48 V/110 Ah lithium batteries, which could support all of the equipment operations without interruption for up to 5 h. The inlet systems for our mobile laboratories were specifically configured to accommodate the type of measurement requirements and the instrument suite to be employed in specific field campaigns.

Instruments deployed on the mobile laboratory included those for studying NO_x, CO, SO_2, BC and ultrafine particles. NO_x was measured using an NO_x analyser with an Mo-converter (Ecotech model 9841A; Ecotech, Knoxfield, Melbourne, Australia). CO was measured with a CO analyser by light absorption (Ecotech model 9830A). SO_2 was measured using an SO_2 analyser with a fluorescence cell (Ecotech model 9850A). BC was measured using a multi-angle absorption photometer (MAAP; Thermo model 5012; Thermo Scientific, Waltham, MA). The precisions, uncertainties and time resolutions of these analysers were shown in table 1. The online measurement data from these instruments were recorded with an industrial personal computer.

123 Table 1. here.

124 Each time before an experiment, we did a calibration to obtain calibration curves, e.
125 g. on June 16 in 2013 (Fig. S2), and after the experiment we did another calibration
126 and recorded the span drifts. The span drifts were less than 10%. For example,
127 according to the calibration on June 23 in 2013, the span drifts of NO, SO_2 and CO
128 were 29 (365) ppb, 9 (160) ppb and 0.1 (7.4) ppm. In previous study we also did
129 inter-comparison with monitoring station in the campus of Peking University (Wang
130 et al., 2009).

131 Ultrafine particles were measured with a fast mobility particle sizer (FMPS, TSI
132 3090; TSI, Shoreview, MN), which covers particle sizes from 5.6 nm to 560 nm in 32
133 channels with a time resolution of 0.1 s. The data were recorded on a dedicated
134 computer. Other auxiliary data including temperature, relative humidity, barometric
135 pressure and GPS coordinates were also measured. The driving speed was kept stable
136 at around 100 ± 5 km h^{-1} to cover as much distance as possible with the 5 h of power
137 supplied by the lithium batteries.

138 To establish the spatial distribution and characterise the regional transport of air
139 pollutants in the NCP, the routes for the mobile measurements were specially designed
140 to cover important emissions hotspots (Fig. 1) and to map large areas of the NCP. The
141 routes included the municipalities of Beijing and Tianjin, most of Hebei province, and
142 part of Shandong province, which is about 300 km wide from the west to the east and
143 400 km long from the north to the south, covering most of the NCP. To avoid traffic

144 jams and rough roads, only expressways were chosen for all routes. Limited by the
145 duration of battery power and the variability of boundary layer height, we could not
146 cover all routes in one trip. Instead, we divided the routes into five parts. Route 1 was
147 along the Taihang Mountains from Beijing to Shijiazhuang, located in the western part
148 of the NCP. Routes 2 and 3 were from Shijiazhuang to Dezhou and Cangzhou to
149 Baoding, respectively, which were generally located in central NCP. Routes 4 and 5
150 were from Tianjin to Beijing and around the south of Beijing, located in northern NCP.
151 In addition, we ran each route in one day. Two days were also needed for calibration
152 and maintenance of instruments. Therefore, it took one whole week to conduct a
153 single experiment. In total, six experiments, including one pre-test study, were
154 designed from June 1 to July 15, 2013. The pre-test study was conducted between
155 June 1 and June 7, and five formal repeated experiments were conducted between
156 June 11 and July 15 (Experiment 1 [E1], June 11–June 15; E2, June 17, June 18 and
157 June 20; E3, June 24–June 25; E4, July 2–July 7; E5, July 11–July 15). All trips were
158 started at about 09:00 and ended at about 14:00 to ensure that the boundary layer was
159 relatively stable during the observation period in 1 day.

160 The major reasons for data lacking were the computer crashing and rain. Rain
161 caused the missing data on route 3, route 4 and route 5 in experiment 3, and on route 5
162 in experiment 5. Computer crashing caused the missing data on route 4 and route 5 in
163 experiment 2 (Table S1). Also, the computer crashing caused data missing during
164 every trip (Table S2)

Figure 1 here.

2.2 The trajectories model

A Lagrangian particle dispersion model, FLEXPART-WRF version 3.1 (Brioude et al., 2013; Stohl et al., 1998; Stohl et al., 2005; Fast and Easter, 2006), was used to determine the origin and transport pathways of the air mass arriving at the vehicle-based mobile measurement laboratory. The wind field used to drive FLEXPART was the time-averaged wind provided by the WRF with temporal intervals of 10 min and horizontally spatial resolution of 2 km (The details of the mesoscale meteorological model is described in S2.1). FLEXPART simulates the transport and dispersion of tracers by calculating the backward trajectories of multitudinous particles, which are termed plume back trajectories. In this model, turbulence in the planetary boundary layer (PBL) is parameterised by solving the Langevin equation, and convection is parameterised using the Zivkovic Rothman scheme (Stohl et al., 2005). To improve the accuracy of the trajectory calculation, we used high-resolution WRF simulation domain 4 outputs as the input meteorological conditions for the FLEXPART model. The turbulence, convection and boundary layer height were computed along the trajectories of tracer particles using the WRF output data. Backward integration was performed every 5 min during the mobile observation period in June 2013. For each integration, 2000 stochastic particles were released initially from within a box 1×1 km^2 in horizontal extent and 1–50 m vertical height above ground centred on the mobile measurement laboratory. A total of 2000 inert

tracer particles were released about every 5 min along the route of the vehicle. For each release, the backward trajectories were simulated for at least 12 h, and the particle locations were output every 10 min for analysis. The 12 h length of the backward trajectories was chosen as a trade-off to adequately sample the history of the air masses over the region of interest, while decreasing the trajectory error (Stohl, 1998; Zhang et al., 2012).

The footprints of backward trajectories were calculated to present plume trajectories. Footprints in this context refer to the total residence times of released particles, which were calculated following Ashbaugh et al. (1985) and de Foy et al. (2009) by counting the accumulated number of particles during the integration within each cell of a 2 × 2 km^2 grid. Various transport and diffusion patterns can well be described by these footprints analyses (Zhang et al., 2012).

2.3 Stationary measurement sites and the fire data

Concentrations of air pollutants, including NO_x, SO_2, CO and BC, were measured simultaneously at three stationary measurement sites during CAREBeijing-NCP 2013. These were rural sites located at Gucheng, Hebei province (GC, 39.13°N, 115.67°E), Quzhou, Hebei province (QZ, 36.78°N, 114.92°E) and Yucheng, Shandong province (YC, 36.67°N, 116. 37°E) (Fig. 1). The GC stationary site was near route 1, and QZ and YC stationary sites were near route 2. The straight-line distances from these stationary sites to the nearest measuring roads were 3 km from GC station to route 1, 54 km from QZ station and 5 km from YC station to route 2. And these stationary data

were hour-average. The concentrations plotted in Fig. 2 were hour-average results when our mobile laboratory passed by these stations. Furthermore, the footprint maps (Fig. 7 and Fig. S6) show the wind directions and wind speeds at these sites.

The main pollutants at these sites were measured using commercial instruments. At the QZ site, gas analysers were used to measure NO_x (Ecotech model 9841A), CO (Ecotech model 9830A) and SO_2 (Ecotech model 9850A). At GC and YC stations, gas analysers were used to measure NO_x (Thermo model 42C), CO (Thermo model 48i) and SO_2 (Thermo model 48i), and BC was measured by MAAP (Thermo model 5012).

Fire data were obtained from the Moderate Resolution Imaging Spectroradiometer (MODIS) installed in Terra and Aura. The territory passing times were 10:30 (local time) and 13:30 (local time) for Terra and Aura, respectively. Fire images were obtained from EOSDIS Worldview (NASA, https://earthdata.nasa.gov/labs/worldview).

3. Result and discussion

3.1 Distribution of air pollutants

BC, NO_x, CO and SO_2 were measured on five routes during the experiment to determine the concentrations of air pollutants on the routes and their spatial distributions in the NCP. Figure 2 shows the results of our mobile measurements obtained in 19 trips on the five routes from June 11 to July 15. The mean and median

concentrations of BC, NO_x, CO and SO_2 were 5.8 and 5.5 μg m^{-3}, 422 and 452 ppb, 1006 and 956 ppb and 15 and 12 ppb, respectively, in the whole study. These high values were consistent with previous measurements of most pollutants at stationary measurement sites in the NCP except for NO_x. For example, the measured concentrations of NO_x, SO_2 and CO were 62.7 ± 4.0 ppb, 31.9 ± 2.0 ppb and 1990 ± 130 ppb in an urban site in the courtyard of China Meteorological Administration in the Beijing area from November 17, 2007, to March 15, 2008 (Lin et al., 2011). These values were 13–50 ppb, 5.7–30.3 ppb and 1100–1800 ppb at an urban site in Wuqing (between Beijing and Tianjin) from July 9, 2009, to January 21, 2010 (Wu et al., 2011); and 28.4 ppb, 17.2 ppb and 1520 ppb at the GC site from July 2006 to September 2007 (Lin et al., 2009). In addition, the concentration of NO_2 measured at the YC site from June 18 to June 30 was about 20 ppb (Wen et al., 2015). This comparison with stationary site measurements suggested that our mobile measurements reflected the heavily polluted conditions in the NCP, which ensured its feasibility in profiling the distributions of these air pollutants.

Figure 2 here

The levels of CO, NO_x and BC here were also comparable to those in previous mobile laboratory measurements in European and American cities. Bukowiecki et al. (2002) measured CO in Zürich, Switzerland, and the average concentration was about 600 ppb. Hagemann et al. (2014) measured NO_x in Karlsruhe in Germany, and the average concentration was about 20 ppb. In the USA, NO_x was around 50 ppb in

Somerville (Padró-Martínez 2012), 200 ppb during rush hour in Boston (Kolb et al., 2004) and ranged from 230 ppb to 470 ppb in Los Angeles (Westerdahl et al., 2005). Padró-Martínez et al. (2012) also measured BC in Somerville, and reported average concentrations of about 1 μg m^{-3}. As these measurements were obtained in heavy-traffic areas in large cities, and our results were measured over a large region, we concluded that the air pollution problems in the NCP are among the worst in the world. In contrast to these pollutants, a low concentration of SO_2 was consistently measured throughout the whole study.

As shown in Figure 3, the concentrations of BC, NO_x, CO and SO_2 were highly variable on the different routes in the NCP. The concentration ranges of these four species were 5–14 μg m^{-3} for BC, 447–891 ppb for NO_x, 22.6–40.4 ppb for SO_2 and 1105–1652 ppb for CO. These extremely high values, i.e., 95 percentile concentrations, were consistently found in various plumes near these emissions hotspots in the NCP, which suggested a major influence on concentrations of measured species in these hotspot areas by local emissions. The hotspots observed here were mainly around the junction areas of our design routes, and they included but were not limited to areas of Beijing, Tianjin, Baoding, Cangzhou, Dezhou, Shijiazhuang and Zhuozhou. Previous model simulations and satellite measurements in the NCP also confirmed the high concentrations of NO_2 around these large cities (Shi et al., 2008). It is worth noting that these observed concentration hotspots moved around the emissions hotspots, probably as a result of the varied transport processes in different trips. For example, a pollution plume was detected 100 km to the south of

Cangzhou on June 20, but 130 km to the north of Cangzhou on July 6. In addition, plumes were not always detected in different experiments around these cities, with the exception of Shijiazhuang.

Figure 3 here.

During the five experiments, no clear temporal distributions of air pollutant concentrations in the NCP were seen, except for the significantly low levels of NO_x and SO_2 observed in the last experiments. However, no connections between the decline in NO_x and SO_2 concentrations and emissions or transport could be made. In fact, precipitation caused the low concentrations of NO_x and SO_2 in the last experiment in NCP. And all measuring areas were affected by heavy rain, so the concentrations of NO_x and SO_2 on all routes were low.

In summary, our mobile laboratory measurements indicated spatial distributions of the pollutants SO_2, CO and BC and the number density of fine particles. The concentrations of air pollutants in the NCP were among the highest in the world and extremely high concentrations were also observed around several cities.

3.2 The influence of traffic emission

The levels and distributions of air pollutants in the NCP are mainly attributable to three sources, i.e., regional transport, local emissions and traffic emissions. On-road measurements, however, could be greatly affected by traffic emissions (Wang et al., 2009). The influence of traffic emissions on our mobile laboratory measurements is

discussed below.

3.2.1 1. Comparing the on- and off-road measurements of air pollutants to estimate the enhancement of air pollution on highway above the regional background

Each on-road measurement trip started from a parking lot in a highway service center and ended at the parking lot of another service center. The parking lots are about 150 m away from highway, such as those in service centers Dezhou (DZ) and Xizhaotong (XZT) (Fig. S3). Using the difference of the concentrations of air pollutants measured in a parking lot and on highway, we can estimate the level of the enhancement of the concentrations of air pollutants on highway above regional backgrounds.

Table 2 shows the 5 min averaged concentrations of NO_x, CO, SO_2, and BC measured in parking lots and on highways, and the difference between the on- and off-road concentrations. The concentrations in parking lots were measured for 5 mins before driving or after parking with engine turned off, and the concentrations on highways were measured for 5 mins after entering highways or 5 mins before entering the service centers.

The concentrations of NO_x measured on highway show drastic enhancement than those measured off-road, from 19 to 449 ppb, or 43% to 1658% (510±61%, mean± Standard deviation), while other pollutants have much lower enhancement or even reduction in concentrations. The difference between the on-road and off-road concentrations of CO ranged from -478 to 145 ppb, or -28% to 34% (7±22%); for SO_2,

311 it is -26 to 13 ppb or -18% to 175% (52±59%); for BC, it is -0.7 to 4.7 g m^{-3} or -11%
312 to 261% (85±90%).

313 The 175% enhancement of SO_2 on July 12 could be due to the much lower SO_2
314 concentration, 1.2 to 3.3 ppb, than those measured in other days. The rain on July 12
315 is likely the major reason for the much lower concentrations of SO_2 (3 ppb) and NO_x
316 (63 ppb), while CO and BC, which are much less water soluble, show no significant
317 difference than those measured in other days. If we ignore the results of SO_2 and NO_x
318 on July 12, then the difference between the on- and off-road concentrations were 82%
319 to 1658% (510±61%) for NO_x and were -18% to 87% (31±31%) for SO_2.

320 Apparently, vehicular emission is the major source lead to the 82% to 1658%
321 enhancement of NO_x concentrations on highway. The enhancement of CO and SO_2
322 concentrations on highway were mostly less than 30%, suggesting vehicular emission
323 is not the main source for CO and SO_2 on highway, regional background is the
324 dominant factor determine their concentrations.

325 **3.2.2 2. Time series of the concentrations of air pollutants measured on highway**

326 Figure 4 shows the concentrations of NO_x, CO, SO_2, and BC measured on highway
327 on a typical day, June 13, 2013. Apparently, the concentration of BC follows the trend
328 of NO_x concentration and those of CO and SO_2 did not. This suggests the high
329 enhancement of NO_x and BC concentration on highway was due to the vehicular
330 emission, while the concentrations of CO, SO_2 were not.

331 Figure 4. here.

3.2.3 Using the ratios of weighted vehicular emission factors to estimate the concentration enhancement of NO_x, CO, SO_2 and BC measured on highway

Based on the reported vehicular emission factors (Shen et al., 2015; Cai and Xie, 2007, 2010; Lei et al., 2011) and the vehicle composition (Chinese Automotive Technology & Research Centre, 2015) in Hebei province, where we conducted the most of the mobile measurements, we estimated the weighted vehicular emission factors on the highways (Table 3). The factors for NO_x, CO, SO_2, and BC during our measurements were 2.9 g km^{-1}, 4.8 g km^{-1}, 0.04 g km^{-1}, and 0.01 g km^{-1}, respectively. If we assumed 400 ppb as the NO_x concentration enhancement on-road caused by vehicular emission, using the ratios of the weighted vehicular emission factors, the estimated enhancements of CO, SO_2 and BC concentrations on-road emitted by vehicles were 240 ppb, 3 ppb and 1 μg m^{-3}. These are at the similar levels of those enhancement showed in Table 1, suggesting vehicular emission is the main source for the enhancement of the on-road concentrations of NO_x, CO, SO_2, and BC. However, the enhancement of CO and SO_2 concentrations on highway were mostly less than 30%, this provides further evidence that CO and SO_2 concentrations on highway were dominated by regional background; and vehicular emission was not the main source.

Table 3. here.

3.2.4 Correlations between NO_x, CO, SO_2 and BC with NO

A strong correlation (r^2 = 0.99) was found between on-road NO_x and NO (Fig. 5), with an average NO/NO_2 ratio of 4, which was much higher than the value of 0.05–

353 0.2 in the aged plumes (Finlayson-Pitts and Pitts, 2010). The results indicated that
354 NO_x observed by our mobile laboratory was mostly influenced by fresh vehicle
355 emissions. Overall, the on-road NO_x observations here were not representative of the
356 NO_x levels in the NCP. While, the concentrations of BC, CO and SO_2 were not
357 correlated with those of NO.

358 Figure 5. here.

359 **3.2.5 Possible traffic jams and high concentrations of air pollutants**

360 Each on-road measurement trip started from a parking lot in a highway service center
361 and ended at the parking lot of another service center. The driven speed of the mobile
362 platform was never lower than 80 km h^{-1} on highways, this is one of the evidences
363 that we encountered no traffic jams, and the number of vehicles around our mobile
364 platform seldom increased.

365 During our measurements, as shown in Fig. 3, we always measured high
366 concentrations of air pollutants near large cities. As the time series of the
367 concentrations of NO_x, CO, SO_2 and BC measured on June 13 (Fig. 6) show, when
368 approaching Baoding, CO concentration gradually increased from 500 ppb at 50 km
369 away from Baoding to 1200 ppb at 23 km away from Baoding. The same is SO_2 (from
370 10 ppb to 40 ppb) and BC (from 4 μg m^{-3} to 8 μg m^{-3}), while NO_x does not show the
371 same trend. When at 15 km away from Baoding, we see another increase of all the
372 pollutants, and the same decrease trend after at 10 km from Baoding. The same
373 continuously increasing trends of SO_2 and CO, started at 50 km to 15 km away from

374 Baoding, indicated the regional transport of SO_2 and CO. Started at 15 km, away from
375 Baoding, all the four pollutants had a peak with about 10 km width, which indicated
376 the urban emissions.

377 Figure 6. here.

378 In summary, both the comparison of on- and off-road measured concentrations and
379 the vehicular emission factors provided the evidences:
380 (1) Vehicular emission is the main source for the enhancement of the on-road
381 concentrations of NO_x, CO, SO_2, and BC;
382 (2) The high enhancement of NO_x concentration on highway suggesting NO_x on
383 highway was mainly from vehicular emission;
384 (3) CO and SO_2 concentration have up to 20% and 31% average enhancement on
385 highway, suggesting that CO and SO_2 on highway were mainly from regional
386 background.
387 (4) The difference in the enhancement is the difference of level of background
388 contribution. NO_x has shorter life time, while the lifetimes of CO and SO_2 in the
389 atmosphere are longer, and regional background contribution become important

390 Thus, the CO and SO_2 measurement results could be used for studying the spatial
391 distributions of the air pollutants in the NCP region. The hot spots measured near
392 large cities were mainly from local emissions.

393 **3.3 The influence of regional transport**

394 Local emissions and regional transport are the two main sources of pollutants in the

NCP (Xu et al., 2011). As stated above, local emissions in large cities had a major impact on the air quality in their adjacent areas. We found all air pollutants measured near large cities were at high level. According to the analyzation in section 3.2, they were mainly from local emissions of cities. Also, according to the estimated emission inventories, these cities were major sources of air pollution which caused the concentrations of air pollution high around them. Regional transport also plays a major role. Our study demonstrated that the contribution of regional transport could vary both spatially and temporally, depending on a number of parameters, such as prevalent wind, terrain and vertical mixing. We also roughly divided the NCP into two parts according to these parameters, i.e., the northern border area and the central area, to discuss the influence of regional transport on air quality. All trip-average concentrations of SO_2, CO and BC and wind directions on those days discussed in the manuscript were shown in table 4.

Table 4. here.

3.3.1 The border areas of NCP

The northern border area of the NCP included major parts of routes 4 and 5 and the western border areas of the NCP included a major part of route 1. The area is surrounded by the Taihang Mountains to the west and the Yan Mountains to the north. The north wind prevailed in the winter and the south wind prevailed in the summer in this area.

During the measurements, the three routes experienced both north and south winds. Specifically, northwest winds and east winds brought outside air masses from Northeast China and the Bohai Sea to the northern border area on July 2 (route 1) and July 7 (route 5), respectively (Fig. 7). In both trips, the concentrations of SO_2, CO and BC were 4.5 ± 2.3 ppb, 550 ± 240 ppb and 5.0 ± 2.6 μg m^{-3}, respectively, on July 2 and 7.0 ± 3.0 ppb, 1090 ± 320 ppb and 6.5 ± 2.7 μg m^{-3}, respectively, on July 7 (Fig. 2), which were the lowest values observed here in the border areas of the NCP. These observations were reasonable as areas including the Bohai Sea to the west, north and east of the NCP were regions of low emissions (Fig. 3) and the clean air brought by northeast and east winds could dilute the air pollutants in the border areas of the NCP.

Figure 7 here.

It is worth noting that the BC concentration was not lowest on July 2, which was the opposite of the observations for the gas pollutants, SO_2 and CO. Satellite images showed that there were many fire plots near route 1 on July 2 (Fig. S4). A featured single peak of aerosol number density at around 50 nm (Fig. S5) further confirmed that BC emissions from agricultural crop residue burning contributed significantly to the BC levels on July 2 (Zhang et al., 2011; Hays et al., 2005; Li et al., 2007).

On June 24 (route 1), June 14 (route 4) and June 15 (route 5), the air masses were transported inside the NCP from the southern NCP to the northern border areas by south winds (Fig. 7). Under these wind conditions, the concentrations of SO_2, CO and BC were 15 ± 5.8 ppb, 1300 ± 330 ppb and 8.0 ± 1.4 μg m^{-3}, respectively, on June 24,

26 ± 7.9 ppb, 1200 ± 230 ppb and 6.5 ± 1.5 μg m^{-3}, respectively, on June 14 and 28 ± 7.1 ppb, 1600 ± 370 ppb and 7.0 ± 1.9 μg m^{-3}, respectively, on June 15 (Fig. 2), which were among the highest levels detected on these routes. According to the emissions inventories (Fig. 3), most emissions hotspots were located in the central and southern parts of the NCP. Pollutants could be easily accumulated in air masses of south and central NCP origin. In addition, the Yan Mountains to the north of the border area stopped the possible transport pathway of these air masses, which further enhanced the accumulation of long-lived air pollutants in the northern border area of the NCP.

Although route 4 on July 6 was under the influence of south winds, as the same route on June 14 (Fig. 7), the concentrations of SO_2 and BC on July 6 were 14 ± 7.6 ppb and 4.6 ± 1.8 μg m^{-3}, respectively, on July 6, which were much lower than the values of 26 ± 7.9 ppb and 6.5 ± 1.5 μg m^{-3}, respectively, on June 14. Meanwhile, the CO levels on these two days were similar. One possible cause of the low concentrations of both SO_2 and BC was the slightly higher boundary layer height on July 6 compared to June 14. The precipitation that occurred on July 6, but not on June 14, appeared to be a more important contributing factor. The solubility of CO is less than that of SO_2. Therefore, the wet deposition lifetime of SO_2 would be much shorter, thus limiting the transport distance of SO_2. Meanwhile, the wet deposition of BC particles would also prohibit its long-range transport. This may explain the similar CO levels and low SO_2 and BC levels on July 6 at the same time.

In conclusion, for the northern border area, local emissions and regional transport

457 from other NCP areas due to south winds were two main sources of long-lived
458 pollutants; both north and east winds had significant dilution effects on the
459 concentrations of gas pollutants. It was based on a general situation that the air quality
460 in the north border of the North China Plain was clean, because the emissions of air
461 pollutants were low in that area (Fig. 3). The wind dependency scatter plots for SO_2
462 were used to show the contribution of regional transport to air pollution in the
463 northern border area of the NCP (Fig. 8). The results indicated that the high
464 concentration was connected to the south wind at a wind speed from 4 to 10 m s^{-1}.
465 Similar results for SO_2 and CO were reported for several sites in the northern NCP
466 (Wu et al., 2011; Lin et al., 2011; Lin et al., 2009). As the south wind usually
467 prevailed in the summer and north wind in the winter, the regional transport of
468 long-lived pollutants within the NCP from the central and southern parts to the
469 northern parts should be prevalent in the summer; while the dilution of air pollutants
470 mainly by north winds and occasionally east winds should be prevalent for the
471 northern parts of the NCP in the winter.

472 Figure 8 here.

473 **3.2.2 The central NCP**

474 The central NCP consisted of routes 2 and 3, where numerous heavily polluted cities
475 are located. The area was surrounded by the Taihang Mountains to the west or
476 emissions hotspots in other directions. While the north wind prevailed in the winter, as
477 for the northern border areas, low pressure prevailed in the summer with south and

478 northeast winds in this area.

479 During the observation period, the measurements along the two routes experienced
480 different wind fields. Route 2 experienced southwest winds on June 12 and July 3,
481 northeast winds on June 18 and a low-pressure system with south and northeast winds
482 on June 25 (Fig. S6). Unlike the northern border area of the NCP where strong north
483 winds had a dilution effect, the concentrations of gas pollutants were mostly high
484 regardless of the wind direction on route 2 in the central NCP, e.g., on June 18 and
485 July 3 (Fig. S6). Generally, our observations were reasonable according to the unique
486 terrain and emissions map in central NCP. Due to the heavy emissions level in the
487 central NCP and surrounding areas, pollutants readily accumulated to high levels on
488 their ways to the central NCP in air masses from all directions, such as the clean air
489 masses from the Bohai Sea, West China and Northeast China, and polluted air masses
490 from Southeast China.

491 The situation was slightly different in areas along route 3, particularly for those off
492 the coast of the Bohai Sea. Route 3 experienced east winds on July 14 (Fig. S6), and
493 the concentrations of pollutants were low (Fig. 2). This was not only because of the
494 wet deposition from the rain on that day, but also the transport of clean air from the
495 Bohai Sea. A featured peak of aerosol number density at around 20 nm (Fig. S5)
496 further confirmed the incoming air from the Bohai Sea (Haaf and Jaenicke, 1980;
497 Hoppel et al., 1986).

498 Vertical mixing can also affect the concentrations of pollutants. For example, while

499 the wind fields were similar on route 3 on June 13 and July 4 (Fig. 9), the
500 concentration of pollutants on June 13 was lower than that on July 4 (Fig. 2). This was
501 because the boundary layer was much higher on June 13 (976 m) than on July 4 (626
502 m), and the strong vertical convection diluted the air pollutants.

503 Specifically, the relative contributions of emissions and regional transport to the
504 local air pollution levels were slightly different on different routes. At the junction of
505 routes 1 and 2 around Shijiazhuang area, the concentrations of air pollutants were
506 always high, except in the last experiment when wet precipitation occurred. The local
507 emissions contributed significantly to the air pollution levels in this area. The city of
508 Shijiazhuang is known as an emissions hotspot with heavy coal consumption.
509 Previous model result showed that Shijiazhuang is an important emissions hotspot of
510 SO_2 even in the whole NCP area (He et al., 2012). Meanwhile, the Taihang Mountains
511 to the west of the city prevented the diffusion of air pollutants. On the other hand,
512 transport convergence in front of the Taihang Mountains and Yan Mountains was
513 proposed in a previous study (Su et al., 2004), as a result of a low-pressure system
514 along the Taihang Mountains and Yan Mountains. Although the transport convergence
515 moved around in the north end, it always passed by the Shijiazhuang area. As shown
516 in Figure 3, high levels of pollutants, particularly relatively long-lived species such as
517 SO_2 and CO, were consistently observed at the western end of route 2 near
518 Shijiazhuang area. Broad peaks of SO_2 and CO concentrations, indicators of regional
519 transport plumes, were present near Shijiazhuang area (Fig. S7).

520 Similar to the situation in Shijiazhuang area, transport convergence would
521 occasionally pass through other cities along routes 2 and 3. In a typical case on June
522 13 (Fig. 9), air masses were transported far from the southwest of the NCP along the
523 transport convergence through Shijiazhuang and reached the area on route 3, with air
524 pollutants accumulating during transport and showing high concentrations.

525 Figure 9 here.

526 Overall, in most areas in central NCP, regional transport would play essential soles
527 in determining the local air pollution levels, although the underlying mechanisms
528 were different for the transport convergence area, central NCP area and coastal area.
529 The wind dependence scatter plots for SO_2 and CO were used as examples to show
530 the contribution of regional transport on air pollution in central NCP (Fig. 8). The
531 results indicated that the prevailing winds were southwest and northeast in central
532 NCP during our observation period. The concentrations of CO were independent of
533 wind direction and wind speed. In addition, the high concentrations of SO_2 were
534 related to southeast winds with high speed, which was about 5–10 m s^{-1}. This may
535 have been because of transport convergence. Due to the strong interaction of different
536 areas in central NCP, emissions control policies must consider the whole emissions
537 budget to achieve the air quality aims.

538 We discussed five impactors: local emission, precipitation, location, wind direction
539 and boundary layer height. The influence of local emission reflected in the spatial
540 distribution of concentrations (Fig. 3). Hot spots were found near cities. However, for

route-average results (Fig. 2), local emission plays a minor role in the distribution of concentrations, because the routes were mainly in suburb. The large reduction in SO_2 and NO_x concentration measured on July 12 along all routes were caused by precipitation. The persistent high concentrations of pollutants in route 2 were associated with the location of it, which was surrounded by high emission areas. Besides the route 2, the different concentrations in one route in different measurements were mainly from different wind directions. And we also found one case that the concentrations changed lot between June 13 and July 4 in route 3 under the similar wind directions. Based on the model results, boundary layer height might explain the change.

4. Conclusion

A mobile laboratory was employed to obtain snapshots of the spatial distributions of air pollutants in the NCP. The concentrations observed were at the highest levels in the world and were distributed unevenly in the NCP. Most high concentrations, i.e., 95 percentile concentrations, of air pollutants were found near emissions hotspots, which suggested the influence of local emissions. However, regional transport of air pollutants was also considered significant in determining the air quality in the NCP. Back trajectory analysis, satellite data and tracer pollutants were combined to recognise various cases of regional transport in both the northern border and central NCP. Where the border areas would occasionally be diluted by winds from outside the NCP, the central NCP was affected by regional transport of air pollutants with a few

562 exceptions, such as when precipitation occurred. To achieve the aims of air quality
563 locally, emissions control policies must consider the whole emissions budget in the
564 NCP.

565

566

567 The English in this document has been checked by at least two professional editors,
568 both native speakers of English. For a certificate, please see:

569 http://www.textcheck.com/certificate/bENNRx

570 **Data availability.** The data of mobile and stationary measurements are available upon
571 requests. Also, we are working on installing a web site in this year. We will provide
572 data of GPS, vehicle speed, meteorology, concentrations of air pollutants.

573 **Author contribution.** T. Zhu, Y. Zhu, Y. Han and W. Chen designed the experiments.
574 T. Zhu secured the research grants. Y. Zhu, Y. Han and W. Chen carried out the
575 experiments. J. Zhang developed the model code and performed the simulations. J.
576 Wang managed the data in the program. J. Liu provided the emission maps. L. Zeng,
577 Y. Wu, X. Wang, W. Wang and J. Chen provided the data of stationary measurements.
578 Y. Zhu analyzed the data with contributions from all co-authors. Y. Zhu prepared the
579 manuscript with helps from T. Zhu, C. Ye and Y. Li.

580 **Acknowledgement.** This study was supported by the National Natural Science

581 Foundation Committee of China (21190051, 41121004, 41421064), the European 7th
582 Framework Programme Project PURGE (265325), the Collaborative Innovation
583 Center for Regional Environmental Quality.

584 5. References

585 An, X., Zhu, T., Wang, Z., Li, C., and Wang, Y.: A modeling analysis of a heavy air
586 pollution episode occurred in Beijing, Atmos. Chem. Phys., 7, 3103–3114, 2007.

587 Ashbaugh, L. L., Malm, W. C., and Sadeh, W. Z.: A residence time probability
588 analysis of sulfur concentrations at Grand Canyon National Park, Atmos. Environ.,
589 19, 1263–1270, 1985.

590 Bechle, M. J., Millet, D. B., and Marshall, J. D.: Effects of income and urban form on
591 urban NO_2: Global evidence from satellites, Environ. Sci. Technol., 45, 4914–4919,
592 doi: 10.1021/es103866b, 2011.

593 Brioude, J., Arnold, D., Stohl, A., Cassiani, M., Morton, D., Seibert, P., Angevine, W.,
594 Evan, S., Dingwell, A., Fast, J., Easter, R., Pisso, I., Burkhart, J. and Wotawa, G.:
595 The Lagrangian particle dispersion model FLEXPART-WRF version 3.1,
596 Geoscientific Model Development, 6, 1889-1904, doi:10.5194/gmd-6-1889-2013,
597 2013.

598 Bucsela, E. J., Krotkov, N. A., Celarier, E. A., Lamsal, L. N., Swartz, W. H., Bhartia,
599 P. K., Boersma, K. F., Veefkind, J. P., Gleason, J. F., and Pickering, K. E.: A new

stratospheric and tropospheric NO_2 retrieval algorithm for nadir-viewing satellite instruments: applications to OMI, Atmos. Meas. Tech., 6, 2607–2626, doi: 10.5194/amtd-6-1361-2013, 2013.

Bukowiecki, N., Dommen, J., Prévôt, A. S. H., Richter, R., Weingartner, E., and Baltensperger, U.: A mobile pollutant measurement laboratory-measuring gas phase and aerosol ambient concentrations with high spatial and temporal resolution, Atmos. Environ., 36, 5569-5579, 2002.

Cai, H. and Xie, S.: Determination of emission factors from motor vehicles under different emission standard in China, Acta Scientiarum Naturalium Universitatis Pekinensis, 46, 319-326, 2010.

Cai, H. and Xie, S.: Estimation of vehicular emission inventories in China from 1980 to 2005, Atmos. Environ., 41, 8963-8979, 2007.

Cao, G., Zhang, X., Wang, Y., Che, H., and Chen, D.: Inventory of black carbon emission from China, Adv. Clim. Change Res., 3, 75-81, 2007.

Chin, M., and Jacob, D. J.: Anthropogenic and natural contributions to tropospheric sulfate: A global model analysis, J. Geophys. Res., 101, 18691-18699, doi: 10.1029/96JD01222, 1996.

Chinese Automotive Technology & Research Centre: China Automotive Industry Yearbook, Tianjin, China, 2015.

619 de Foy, B., Zavala, M., Bei, N., and Molina, L.: Evaluation of WRF mesoscale
620 simulations and particle trajectory analysis for the MILAGRO field campaign,
621 Atmos. Chem. Phys, 9, 4419-4438, 2009.

622 Ding, A., Wang, T., Xue, L., Gao, J., Stohl, A., Lei, H. C., Jin, D. Z., Ren, Y., Wang,
623 X. Z., Wei, X. L., Qi, Y. B., Liu, J., and Zhang, X. Q.: Transport of north China air
624 pollution by midlatitude cyclones: Case study of aircraft measurements in summer
625 2007, J. Geophys. Res., 114, D11399, doi:10.1029/2009JD012339, 2009.

626 Ding, K., Liu, J., Ding, A., Liu, Q., Zhao, T., Shi, J., Han, Y., Wang, H., and Jiang, F.:
627 Uplifting of carbon monoxide from biomass burning and anthropogenic sources to
628 the free troposphere in East Asia, Atmos. Chem. Phys., 15, 2843–2866, 2015.

629 Donkelaar, V. A., Martin, R. V., Brauer, M., Kahn, R., Levy, R., Verduzco, C., and
630 Villeneuve, P. J.: Global estimates of ambient Fine particulate matter concentrations
631 from satellite-based aerosol optical depth: development and application, Environ.
632 Health Perspect., 118, 847-855, doi: 10.1289/ehp.0901623, 2010.

633 Fast, J. D. and Easter, R. C.: A Lagrangian particle dispersion model compatible with
634 WRF, in: 7th WRF User's Workshop, NCAR, P6-02, 19–22 June, Boulder,
635 Colorado, 2006.

636 Finlayson-Pitts, B. J. and Pitts, J. N.: Chemistry of the upper and lower atmosphere,
637 Academic press, San Diego, California, USA, 2010.

638 Haaf, W., and Jaenicke, R.: Results of improved size distribution measurements in the
639 Aitken range of atmospheric aerosols, J. Aerosol Sci., 11, 321–330, doi:
640 10.1016/0021-8502(80)90106-8, 1980.

641 Hagemann, R., Corsmeier, U., Kottmeier, C., Rinke, R., Wieser, A., and Vogel, B.:
642 Spatial variability of particle number concentrations and NOx in the Karlsruhe
643 (Germany) area obtained with the mobile laboratory 'AERO-TRAM', Atmos.
644 Environ., 94, 341-352, doi: 10.1016/j.atmosenv.2014.05.051, 2014.

645 He, H., Li, C., Loughner, C. P., Li, Z., Krotkov, N. A., Yang, K., Wang, L., Zheng, Y.,
646 Bao, X., Zhao, G., and Dickerson, R. R.: SO_2 over central China: Measurements,
647 numerical simulations and the tropospheric sulfur budget, J. Geophys. Res., 117,
648 D00K37, doi: 10.1029/2011JD016473, 2012.

649 Hoppel, W. A., Frick, G. M., and Larson, R. E.: Effect of nonprecipitating clouds on
650 the aerosol size distribution in the marine boundary layer, Geophys. Res. Lett., 13,
651 125–128, doi: 10.1029/GL013i002p00125, 1986.

652 Hu J., Wang Y., Ying Q., and Zhang H.: Spatial and temporal variability of $PM_{2.5}$ and
653 PM_{10} over the North China Plain and the Yangtze River Delta, China, Atmos.
654 Environ., 95, 598-609, 2014.

655 Huang, K., Zhuang, G., Lin, Y., Li, J., Sun, Y., Zhang, W., and Fu, S.: Relation
656 between optical and chemical properties of dust aerosol over Beijing, China, J.
657 Geophys. Res., 115, doi: 10.1029/2009JD013212, 2010.

658 Johansson, M., Galle, B., Yu, T., Tang, L., Chen, D., Li, H., Li, J., and Zhang, Y.:
659 Quantification of total emission of air pollutants from beijing using mobile
660 mini-doas, Atmos. Environ., 42, 6926–6933, doi: 10.1016/j.atmosenv.2008.05.025,
661 2008.

662 Kolb, C., Herndon, S., Mcmanus, J. B., Shorter, J., Zahniser, M., Nelson, D., and
663 Jayne, J., Canagaratna, M. R., and Worsnop, D. R.: Mobile laboratory with rapid
664 response instruments for real-time measurements of urban and regional trace gas
665 and particulate distributions and emission source characteristics, Environ. Sci.
666 Technol. 38, 5694-5703, doi: 10.1021/es030718p, 2004.

667 Lei, Y., Zhang, Q., He, K., Streets, D. G.: Primary anthropogenic aerosol emission
668 trends for China, 1990-2005, ACPD, 11, 931-954, 2011.

669 Li, A., Xie, P., Liu, W., Liu, J., and Dou, K.: Studies on the determination of the flux
670 of gaseous pollutant from an area by passive differential optical absorption
671 spectroscopy, (in Chinese), Spectrosc. Spect. Analys., 29, 28–32, doi:
672 10.3964/j.issn.1000-0593(2009)01-0028-05, 2009.

673 Lin, W., Xu, X., Ge, B., and Liu, X.: Gaseous pollutants in Beijing urban area during
674 the heating period 2007–2008: variability, sources, meteorological, and chemical
675 impacts, Atmos. Chem. Phys., 11, 8157–8170, 2011.

676 Lin, W., Xu, X., Ge, B., and Zhang, X.: Characteristics of gaseous pollutants at
677 Gucheng, a rural site southwest of Beijing, J. Geophys. Res., 114, doi:

678 10.1029/2008JD010339, 2009.

679 Liu, X., Li, J., Qu, Y., Han, T., Hou, L., Gu, J., Chen, C., Yang, Y., Liu, X., Yang, T.,
680 Zhang, Y., Tian, H., and Hu, M.: Formation and evolution mechanism of regional
681 haze: a case study in the megacity Beijing, China, Atmos. Chem. Phys., 13,
682 4501-4514, 2013.

683 Meng, Z., Xu, X., Yan, P., Ding, G., Tang, J., Lin, W., Xu, X., and Wang, S.:
684 Characteristics of trace gaseous pollutants at a regional background station in
685 Northern China, Atmos. Chem. Phys., 9, 927–936, 2009.

686 Padró-Martínez, L. T., Patton, A. P., Trull, J. B., Zamore, W., Brugge, D., and Durant,
687 J. L.: Mobile monitoring of particle number concentration and other traffic-related
688 air pollutants in a near-highway neighborhood over the course of a year, Atmos.
689 Environ., 61, 253-264, 2012.

690 Peters, J., Theunis, J., Poppel, M. V., and Berghmans, P.: Monitoring PM_{10} and
691 Ultrafine Particles in Urban Environments Using Mobile Measurements, Aerosol
692 Air Qual. Res., 13, 509–522, doi: 10.4209/aaqr.2012.06.0152, 2013.

693 Qu, L., Li, M., Chen, D., Lu, K., Jin, T., and Xu. X.: Multivariate analysis between
694 driving condition and vehicle emission for light duty gasoline vehicles during rush
695 hours, Atmos. Environ., 110, 103-110, 2015.

696 Shen, X., Yao, Z., Zhang, Q., Wagner, D. V., Huo, H., Zhang, Y., Zheng, B., and He,

697 K.: Development of database of real-world diesel vehicle emission factors for
698 China, J. Environ. Sci., 31, 209–220, doi: 10.1016/j.jes.2014.10.021, 2015.

699 Shen, X., Sun, J., Zhang, Y., Wehner, B., Nowak, A., Tuch, T., Zhang, X., Wang, T.,
700 Zhou, H., Zhang, X., Dong, F., Birmili, W., and Wiedensohler, A.: First long-term
701 study of particle number size distributions and new particle formation events of
702 regional aerosol in the North China Plain, Atmos. Chem. Phys., 11, 1565–1580,
703 2011.

704 Shi, C., Fernand, H. J. S., Wang, Z., An, X., and Wu, Q.: Tropospheric NO_2 columns
705 over East Central China: Comparisons between SCIAMACHY measurements and
706 nested CMAQ simulations, Atmos. Environ., 42, 7165–7173, 2008.

707 Stohl, A., Forster, C., Frank, A., Seibert, P., and Wotawa, G.: Technical note: The
708 Lagrangian particle dispersion model FLEXPART version 6.2, Atmos. Chem. Phys.,
709 5, 2461–2474, 2005.

710 Stohl, A.: Computation, accuracy and applications of trajectories – A review and
711 bibliography, Atmos. Environ., 32, 947–966, 1998.

712 Streets, D. G., Canty, T., Carmichael, G. R., Foy, B. D., Dickerson, R. R., Duncan, B.
713 N., Edwards, D. P., Haynes, J. A., Henze, D. K., Houyoux, M. R., Jacob, D. J.,
714 Krotkov, N. A., Lamsal, L. N., Liu, Y., Lu, Z. F., Martin, R. V., Pfister, G. G.,
715 Pinderm, R. W., Salawitch, R. J., and Wecht, K. J.: Emissions estimation from
716 satellite retrievals: A review of current capability, Atmos. Environ., 77, 1011-1042,

2013.

Su, F., Ren Z., Gao, Q., and Zhang Z.: Convergence System of Air Contamination in Boundary Layer above Beijing and North China: Transport Convergence in Boundary Layer, Res. Environ. Sci., 17, 21-25, doi：10.13198/j.res.2004.01.23.sufq.004, 2004.

Wang Y., Yao L., Wang L., Liu Z., Ji D., Tang G., Zhang J., Sun Y., Hu B., and Xin J.: Mechanism for the formation of the January 2013 heavy haze pollution episode over central and eastern China, Sci. China (Earth Sci.), 57, 14-25, doi: 10.1007/s11430-013-4773-4, 2014.

Wang, M., Zhu, T., Zhang, J., Zhang, Q., Lin, W., Li, Y., and Wang, Z.: Using a mobile laboratory to characterize the distribution and transport of sulfur dioxide in and around Beijing, Atmos. Chem. Phys., 11, 11631–11645, 2011.

Wang, M., Zhu, T., Zheng, J., Zhang, R., Zhang, S., Xie, X., Han, Y., and Li, Y.: Use of a mobile laboratory to evaluate changes in on-road air pollutants during the Beijing 2008 Summer Olympics, Atmos. Chem. Phys., 9, 8247–8263, 2009.

Wang, X., Westerdahl, D., Hu, J., Wu, Y., Yin, H., Pan, X., and Zhang, K.: On-road diesel vehicle emission factors for nitrogen oxides and black carbon in two Chinese cities, Atmos. Environ., 46, 45-55, 2012.

Wang, X., Westerdahl, D., Wu, Y., Pan, X., and Zhang, K.: On-road emission factor

736 distributions of individual diesel vehicles in and around Beijing, China, Atmos.
737 Environ., 45, 503-513, 2011.

738 Wang, Z., Hu, M., Sun, J., Wu, Z., Yue, D., Shen, X., Zhang, Y., Pei, X., Cheng, Y.,
739 and Wiedensohler, A.: Characteristics of regional new particle formation in urban
740 and regional background environments in the North China Plain, Atmos. Chem.
741 Phys., 13, 12495–12506, 2013.

742 Wei, P., Cheng, S., Li, J., and Su, F.: Impact of boundary-layer anticyclonic weather
743 system on regional air quality, Atmos. Environ., 45, 2453-2463, 2011.

744 Wehner, B., Birmili, W., Gnauk, T., and Wiedensohler, A.: Particle number size
745 distributions in a street canyon and their transformation into the urban-air
746 background: measurements and a simple model study, Atmos. Environ., 36,
747 2215-2223, 2002.

748 Westerdahl, D., Fruin, S., Sax, T., Fine, P., and Sioutas, C.: Mobile platform
749 measurements of ultrafine particles and associated pollutant concentrations on
750 freeways and residential streets in Los Angeles, Atmos. Environ., 39, 3597-3610,
751 2005.

752 Westerdahl, D., Wang, X., Pan, X., and Zhang, K.: Characterization of on-road
753 vehicle emission factors and microenvironmental air quality in Beijing, China,
754 Atmos. Environ., 43, 697-705, 2009.

Xu, W., Zhao, C., Ran, L., Deng, Z., Liu, P., Ma, N., Lin, W., Xu, X., Yan, P., He, X., Yu, J., Liang, W., and Chen, L.: Characteristics of pollutants and their correlation to meteorological conditions at a suburban site in the North China Plain, Atmos. Chem. Phys., 11, 4353–4369, 2011.

Xu, W., Zhao, C., Ran, L., Lin, W., Yan, P., and Xu, X.: SO_2 noontime-peak phenomenon in the North China Plain, Atmos. Chem. Phys., 14, 7757–7768, 2014.

Yao, X., Lau, N. T., Fang, M., and Chan, C.: Real-time observation of the transformation of ultrafine atmospheric particle modes, Aerosol Sci. Tech., 39, 831-841, doi: 10.1080/02786820500295248, 2005.

Ying, Q., Wu, L., and Zhang, H.: Local and inter-regional contributions to $PM_{2.5}$ nitrate and sulfate in China, Atmos. Environ., 94, 582-592, 2014.

Yu, F., Luo, G., Bates, T. S., Anderson, B., Clarke, A., Kapustin, V., Yantosca, R. M., Wang, Y., and Wu, S.: Spatial distributions of particle number concentrations in the global troposphere: Simulations, observations, and implications for nucleation mechanisms, J. Geophys. Res., 115, D17205, doi: 10.1029/2009JD013473, 2010.

Zhang, J., Zhu, T., Zhang, Q., Li, C., Shu, H., Ying, Y., Dai, Z., Wang, X., Liu, X., Liang, A., Shen, H. and Yi, B.: The impact of circulation patterns on regional transport pathways and air quality over Beijing and its surroundings, Atmos. Chem. Phys., 12, 5031-5053, 2012.

774 Zhang, Q., Ma, X., Tie, X., Huang, M., Zhao, C.: Vertical distributions of aerosols
775 under different weather conditions: Analysis of in-situ aircraft measurements in
776 Beijing, China, Atmos. Environ., 43, 5526–5535, 2009.

777 Zhang, Q., Quan, J., Tie, X., Huang, M., and Ma, X.: Impact of aerosol particles on
778 cloud formation: Aircraft measurements in China, Atmos. Environ., 45, 665-672,
779 2011.

780 Zhang, W., Zhu, T., Yang, W., Bai, Z., Sun, Y., Xu, Y., Yin, B., and Zhao, X.:
781 Airborne measurements of gas and particle pollutants during CAREBeijing-2008,
782 Atmos. Chem. Phys., 14, 301–316, 2014.

783 Zhang, Y., Hua, M., Zhong, L., Wiedensohler, A., Liu, S., Andreae, M. O., Wang, W.,
784 Fan, S.: Regional Integrated Experiments on Air Quality over Pearl River Delta
785 2004 (PRIDE-PRD2004): Overview, Atmos. Environ., 42, 6157–6173, 2008.

786 Zhao, B., Wang, S., Wang, J., Fu, J., Liu, T., Xu, J., Fu, X., and Hao, J.: Impact of
787 national NO_x and SO_2 control policies on particulate matter pollution in China,
788 Atmos. Environ., 77, 453-463, 2013.

789

790 Table 1. Precisions and uncertainties of air pollutants analyzers used in our
791 experiments

	NO_x	CO	SO_2	BC
Precision	1%	1%	0.5%	0.1 μg m^{-3}
Uncertainty	<10%	<100 ppb	<10%	<1%

Time resolution	30 s	40 s	120 s	6 s

792

793 Table 2. The concentrations of NO_x, CO, SO_2 and BC measured in parking lots and
794 high ways, and the concentration differences between off-road and on-road
795 measurement.

Date	Parking lot	Concentrations							
		NO_x (ppb)				CO (ppb)			
		Off-road (C1)	On-road (C2)	C2-C1	$\frac{C2-C1}{C1}$	Off-road (C1)	On-road (C2)	C2-C1	$\frac{C2-C1}{C1}$
6/11	XZT	234	643	409	175%	694	677	-17	-2%
6/12	XZT	411	699	288	70%	1050	1098	48	5%
6/12	DZ	20	106	86	430%	396	506	110	28%
6/13	DZ	19	334	315	1658%	431	576	145	34%
6/17	XZT	30	297	267	890%	1000	1086	86	9%
6/18	XZT	109	468	359	329%	1212	955	-257	-21%
6/18	DZ	372	677	305	82%	588	711	123	21%
7/3	XZT	49	498	449	916%	826	861	35	4%
7/12	XZT	44	63	19	43%	1708	1230	-478	-28%

796 Table 2 (continuous). The concentrations of NOx, CO, SO_2 and BC measured in
797 parking lots and high ways, and the concentration differences between off-road and
798 on-road measurement.

Date	Parking lot	Concentrations							
		SO_2 (ppb)				BC (μg m^{-3})			
		Off-road (C1)	On-road (C2)	C2-C1	$\frac{C2-C1}{C1}$	Off-road (C1)	On-road (C2)	C2-C1	$\frac{C2-C1}{C1}$
6/11	XZT	11.3	12.7	1.4	12%	2.3	5.6	3.3	143%
6/12	XZT	24.4	30.9	6.5	27%	2.9	6.6	3.7	128%
6/12	DZ	8.9	10.0	1.1	12%	1.5	4.1	2.6	173%
6/13	DZ	14.6	12	-2.6	-18%	2.3	3.6	1.3	57%
6/17	XZT	11	17	6	55%	3.4	5.5	2.1	62%
6/18	XZT	15	28	13	87%	6.6	5.9	-0.7	-11%
6/18	DZ	17	21	4	24%	7.4	10.3	2.9	39%
7/3	XZT	17	21.9	4.9	29%	1.8	6.5	4.7	261%
7/12	XZT	1.2	3.3	2.1	175%	5.3	6.2	0.9	17%

799 Table 3. Estimated weighted vehicular emission factors of CO, NO_x, SO_2 and BC
800 during mobile measurements in Hebei Province, China.

Vehicle type	Composition	Emission factors			
		CO[1] g km^{-1}	NO_x[1] g km^{-1}	SO_2[2] g km^{-1}	BC[3] g km^{-1}

Diesel bus	20%	1.2	11	-	-
Medium-duty diesel vehicles	20%	1.5	6.4	-	-
Light-duty gasoline vehicles	50%	4.4	1.3	-	-
Heavy-duty vehicles	10%	1.6	6.6	0.4	0.11
Weighted emission factor		**2.9**	**4.8**	**0.04**	**0.01**

[1] Shen et al., 2015; [2] Cai and Xie, 2007; [3] Lei et al., 2011

Table 4. Trip-average concentrations of SO_2, CO and BC and wind directions on those days discussed in the manuscript

Route	Date	Concentrations (mean ± SD, ppb)			Wind directions
		SO_2	CO	BC	
Route 1	July 2	4.5±2.3	550±240	5.0±2.6	northwest
Route 5	July 7	7.0±3.0	1090±320	6.5±2.7	east
Route 1	June 24	15±5.8	1300±330	8.0±1.4	south
Route 4	June 14	26±7.9	1200±230	6.5±1.5	south
Route 5	June 15	28±7.1	1600±370	7.0±1.9	south
Route 4	July 6	14±7.6	1100±450	4.6±1.8	south
Route 2	June 12	26±11	950±440	4.8±2.2	southwest
Route 2	June 18	27±10	1030±530	6.8±2.3	northwest
Route 2	June 25	27±16	1020±680	6.5±3.3	stable
Route 2	July 3	23±15	989±450	5.7±2.6	southwest

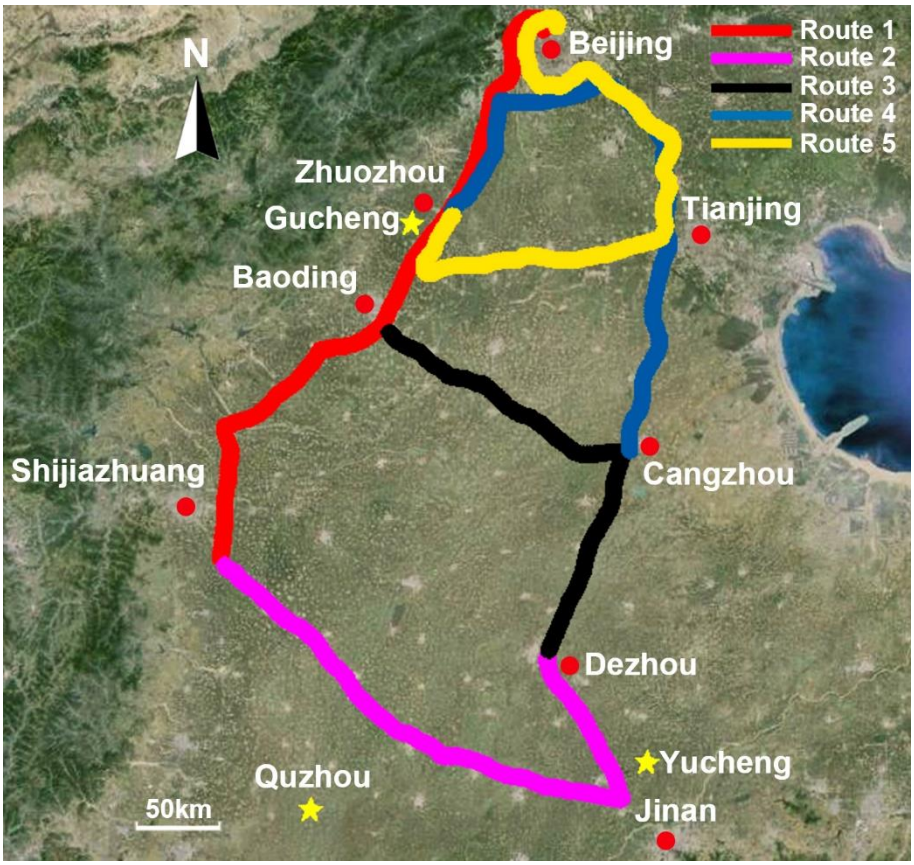

Fig. 1. The study area in NCP. The red track shows route 1, from Beijing to Shijiazhuang. The purple track shows route 2, from Shijiazhuang to Dezhou. The black track shows route 3, from Dezhou to Baoding. The blue track shows route 4, from Cangzhou to Zhuozhou. The yellow track shows route 5, from Zhuozhou to Beijing. The red round dots on the map present the major cities near the routes. The yellow five-pointed stars present the monitoring sites.

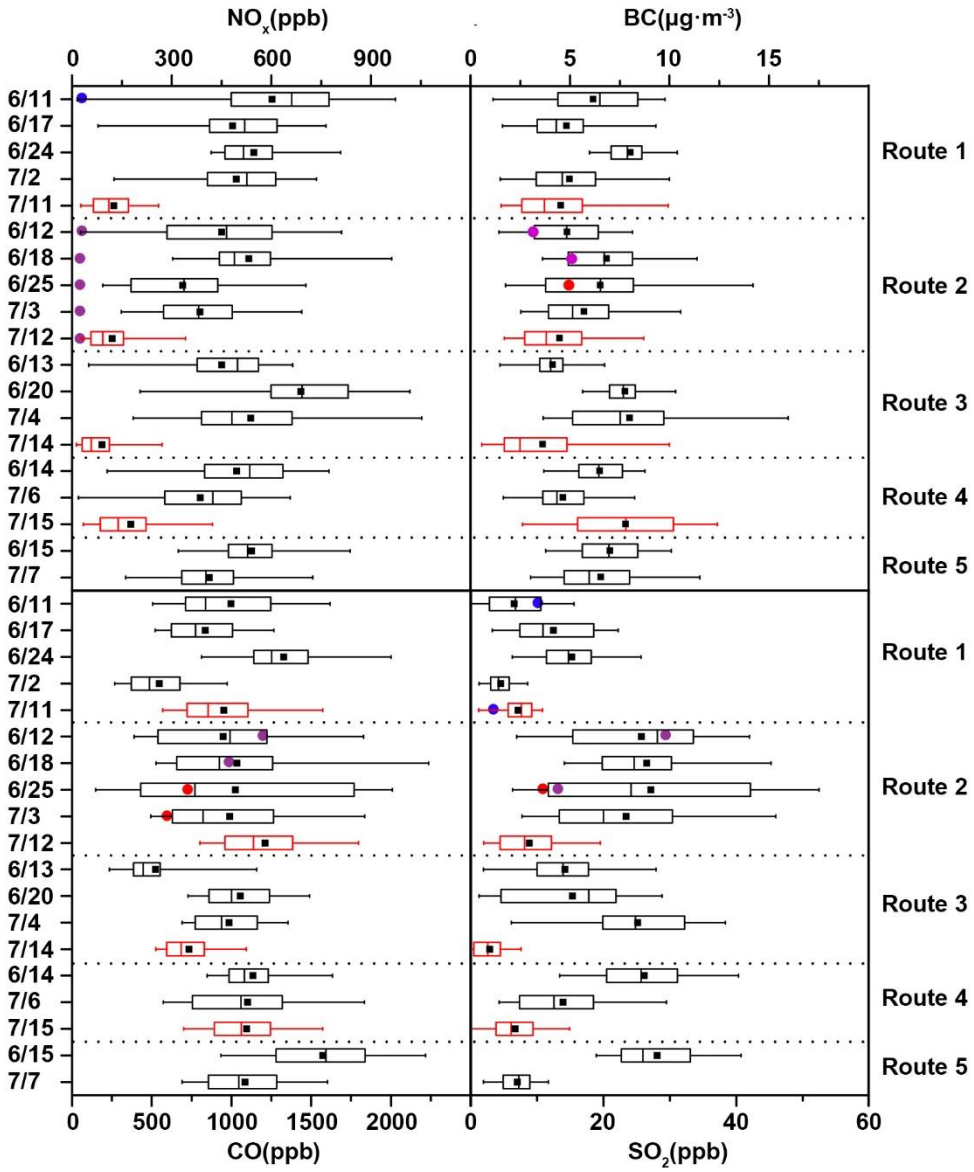

811

812 **Fig. 2.** The concentrations of SO_2, CO, BC and NO_x in each trip in different routes. The red boxes

813 were the results in the last experiment. Values marked were the 5th and 95th percentile (-), standard

814 deviation (lower and upper box lines), median (middle box line), and mean (■). The blue dots

815 were results of GC station. The purple dots were results of QZ station. And the red dots were

816 results of YC station.

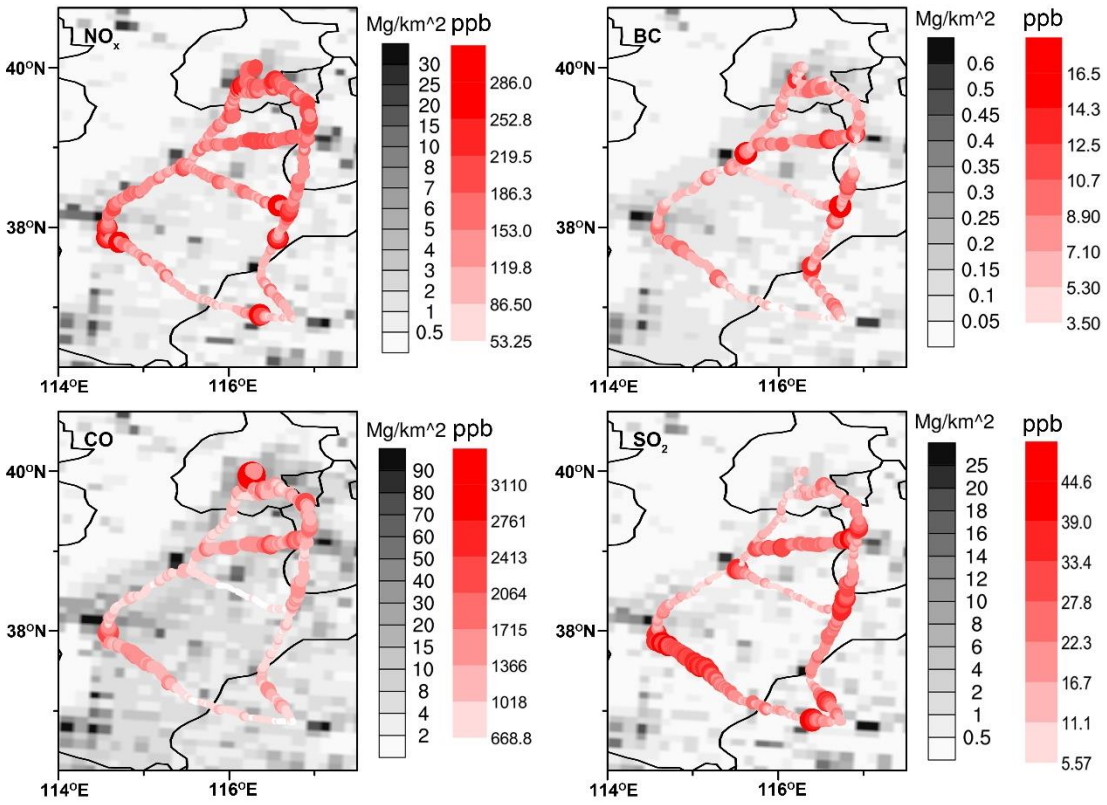

817

818 **Fig. 3.** The spatial distributions of the measured concentrations in our study and the emission

819 maps of SO_2, NO_x, CO and BC. The colored tracks were average concentrations measured in this

820 mobile observation. The black and white maps were emission maps of the year 2010 derived from

821 MEIC model (Zhao et al, 2013).

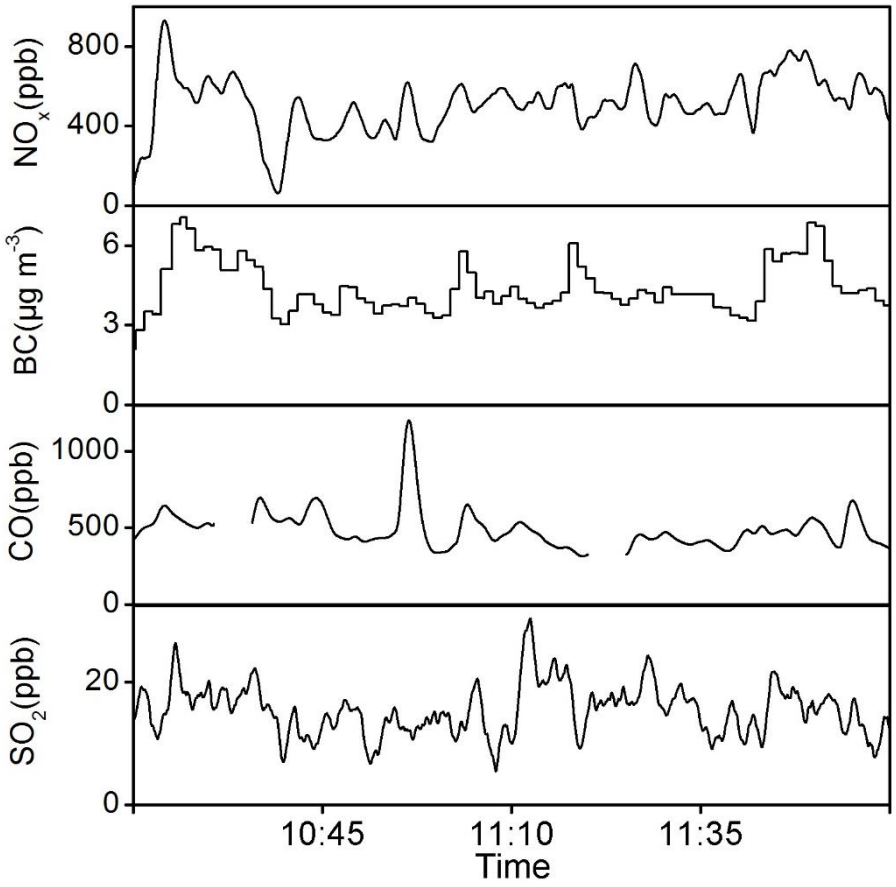

822

823 **Fig. 4.** The time series of the concentrations of NO_x, CO, SO_2 and BC measured on June 13.

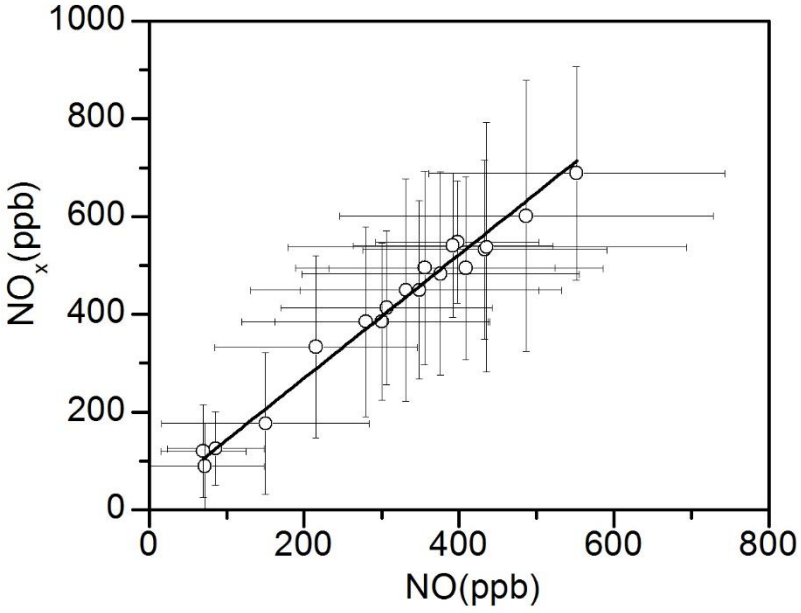

824

825 **Fig. 5.** The regression curve of the means of concentrations of NO_x and NO and the error bars in

826 all 19 trips.

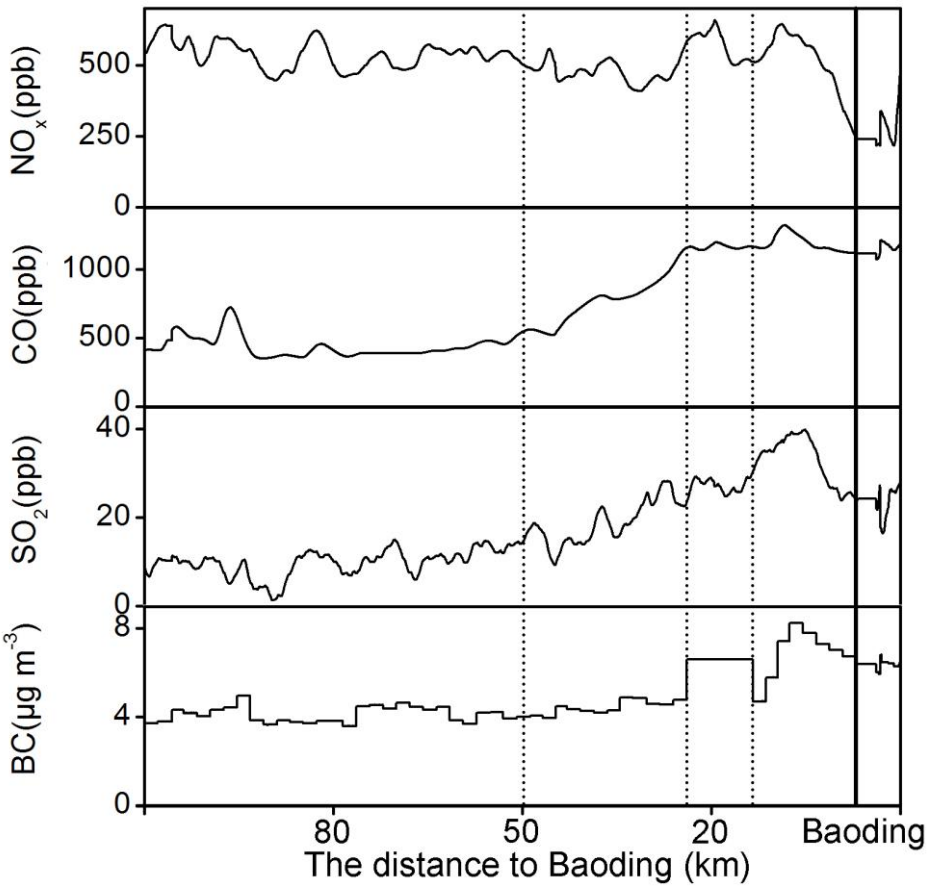

827

828 **Fig. 6.** The time series of the concentrations of NO_x, CO, SO_2 and BC measured on June 13 (the
829 four dashed lines marked the 50 km, 23 km, 15 km to Baoding and Baoding).

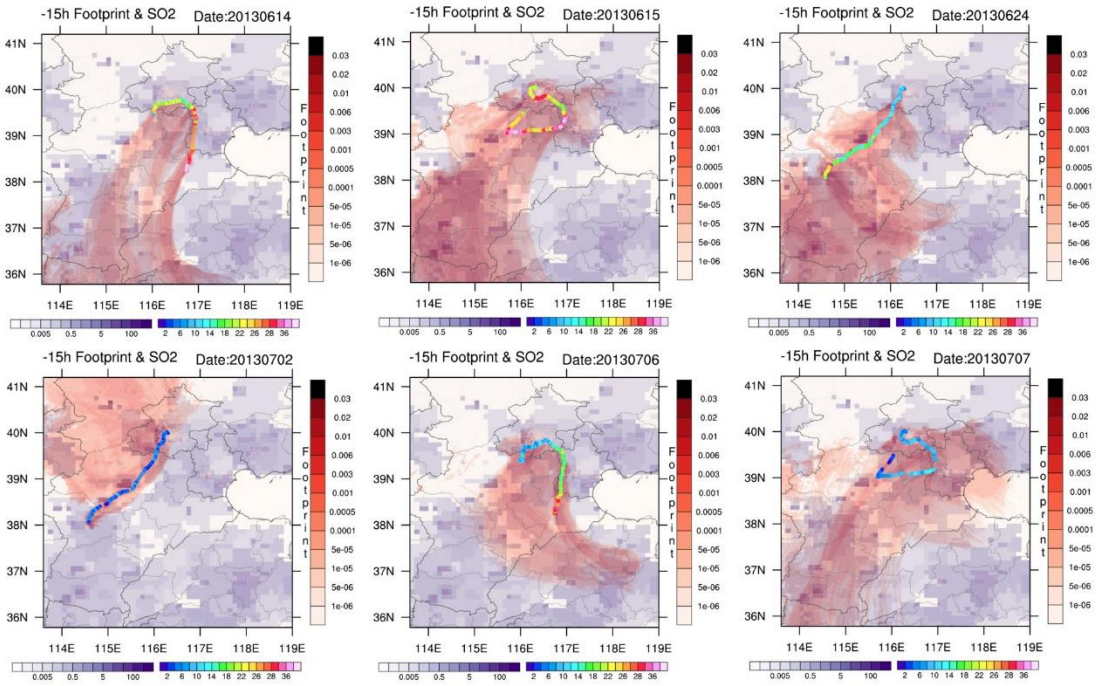

830

831 **Fig. 7.** The back trajectories of observed air masses in the borders of NCP in June 14, June 15,

832 June 24, July 2, July 6 and July 7.

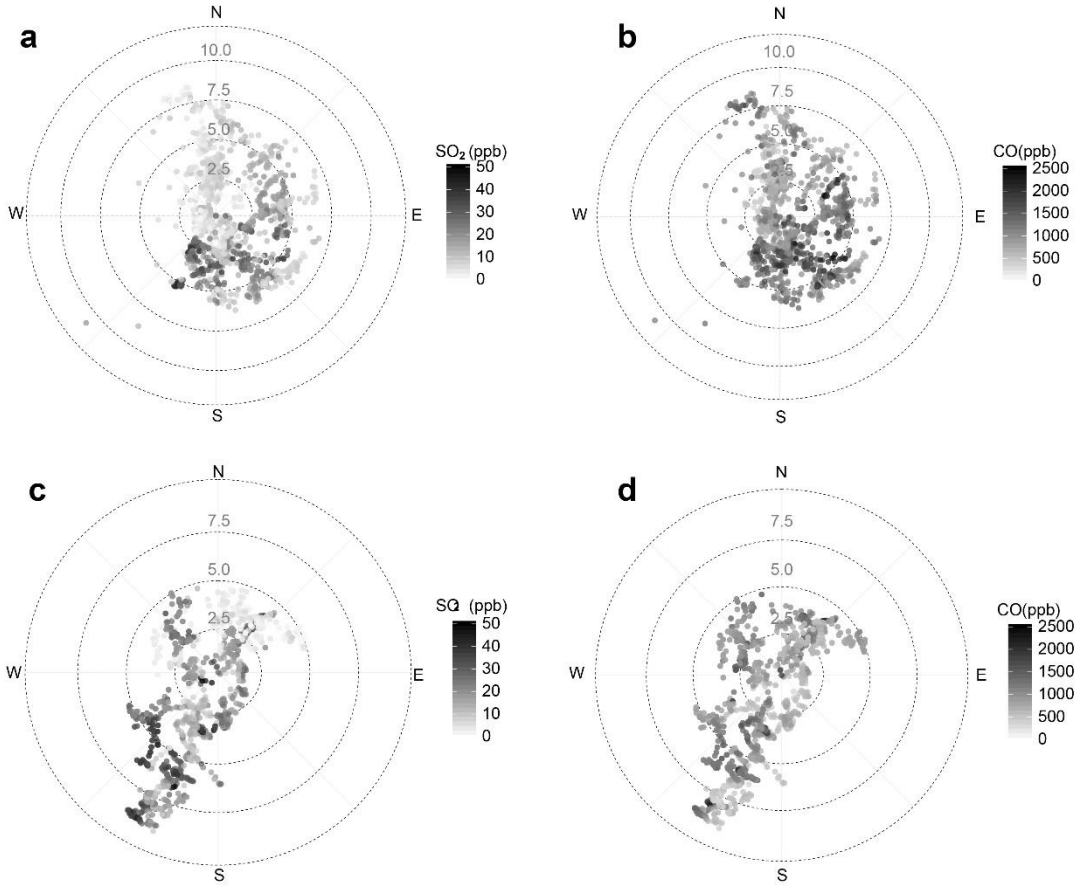

833

834 **Fig. 8.** Wind dependency scatter plots of concentrations of SO_2 and CO in border and central areas

835 in NCP (a. SO_2 in border area; b. CO in border area; c. SO_2 in central area; d. CO in central area).

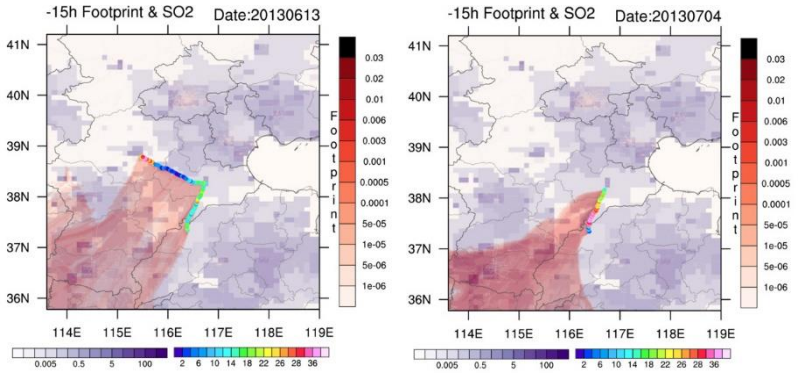

836

837 **Fig. 9.** The back trajectories of observed air masses in the central NCP in June 13 and July 4.

838